Magnon excitations and quantum critical behavior of the ferromagnet $U_4Ru_7Ge_6$

M. P. Nascimento,[1] M. A. Continentino,[1,*] A. López,[2] Ana de Leo,[2] D. C. Freitas,[3] J. Larrea,[1,4] Carsten Enderlein,[5]
J. F. Oliveira,[1] E. Baggio-Saitovitch,[1] Jiří Pospíšil,[6] and M. B. Fontes[1]

[1]*Centro Brasileiro de Pesquisas Físicas, 22290-180 Rio de Janeiro, Brazil*
[2]*Instituto de Física, Universidade do Estado do Rio de Janeiro, 20550-900, Rio de Janeiro, RJ, Brazil*
[3]*Instituto de Física, Universidade Federal Fluminense, 24210-346 Niterói, Rio de Janeiro, Brazil*
[4]*Instituto de Física, Universidade de São Paulo, 05508-090 São Paulo, São Paulo, Brazil*
[5]*Campus de Duque de Caxias, Universidade Federal do Rio de Janeiro, Estrada de Xerém 27, 25245-390 RJ, Brazil*
[6]*Faculty of Mathematics and Physics, Charles University, DCMP, Ke Karlovu 5, CZ-12116 Praha 2, Czech Republic*

We present an extensive study of the ferromagnetic heavy-fermion compound $U_4Ru_7Ge_6$. Measurements of electrical resistivity, specific heat, and magnetic properties show that $U_4Ru_7Ge_6$ orders ferromagnetically at ambient pressure with a Curie temperature $T_C = 6.8 \pm 0.3$ K. The low-temperature magnetic behavior of this soft ferromagnet is dominated by the excitation of gapless spin-wave modes. Our results on the transport properties of $U_4Ru_7Ge_6$ under pressures up to 2.49 GPa suggest that $U_4Ru_7Ge_6$ has a putative ferromagnetic quantum critical point (QCP) at $P_c \approx 1.7 \pm 0.02$ GPa. In the ordered phase, ferromagnetic magnons scatter the conduction electrons and give rise to a well-defined power law temperature dependence in the resistivity. The coefficient of this term is related to the spin-wave stiffness, and measurements of the very low temperature resistivity show the behavior of this quantity as the ferromagnetic QCP is approached. We find that the spin-wave stiffness decreases with increasing pressure, implying that the transition to the nonmagnetic Fermi liquid state is driven by the softening of the magnons. The observed quantum critical behavior of the magnetic stiffness is consistent with the influence of disorder in our system. At quantum criticality ($P = P_c \approx 1.7 \pm 0.02$ GPa), the resistivity shows the behavior expected for an itinerant metallic system near a ferromagnetic QCP.

DOI: 10.1103/PhysRevB.98.174431

I. INTRODUCTION

The problems related to strongly correlated electronic systems are of great current interest due to the novel states of matter that can arise in these systems [1–4]. These include their exotic magnetic properties, their superconducting behavior, and their phase diagrams, which exhibit quantum critical points (QCPs) [5]. QCPs are experimentally explored by doping, applied pressure, or magnetic field [1]. In the case of actinide materials, the interesting properties arise from partially filled f orbitals that strongly hybridize with the conduction electrons. This, together with the strong correlations among the f states, gives rise to a variety of ground states.

The ternary compound $U_4Ru_7Ge_6$ is a system with interesting magnetic properties. It has a centered-body (bcc) crystalline structure of the type $U_4Re_7Si_6$ [6]. The lattice parameter is $a = 8.287$ Å, and the interatomic space between the uranium atoms is $d_{U-U} = 5.864$ Å [7], which is much larger than the Hill boundary for uranium: $d_{U-U} = 3.4$– 3.6 Å, which sets conditions for a magnetic ground state [8]. The compound $U_4Ru_7Ge_6$ has the properties of a heavy-fermion system, with a Kondo resistivity and a large linear term in the low-temperature specific heat [7]. It orders ferromagnetically at low temperatures due to the small volume of its

unit cell, which favors the Ruderman-Kittel-Kasuya-Yosida interaction [7,9,10]. Its ferromagnetism is characterized as itinerant, although Mentink *et al.* [7] propose localized ferromagnetism, contrary to other works in the literature [11–13]. Under applied pressure, transport measurements show no evidence of discontinuous behavior as the ferromagnetic phase is suppressed and a nonmagnetic Fermi liquid state is attained [12].

In this work, we present an extensive study of the magnetic, thermodynamic, and transport properties of $U_4Ru_7Ge_6$ [13,14] under external magnetic fields. The transport properties are also studied for different applied pressures. We show that this system, below its ambient pressure ferromagnetic transition at $T_C = 6.8 \pm 0.3$ K, has its low temperature properties dominated by the presence of low-energy spin-wave excitations. In systems with strong magnetocrystalline anisotropy such as compounds containing f states, these modes are generally quenched at low temperatures by the existence of a gap in the spin-wave spectrum due to this anisotropy. However, $U_4Ru_7Ge_6$ is a unique system among the actinide materials with a negligible magnetocrystalline anisotropy [13,14]. This allows for the excitation of magnons at very low temperatures, and these modes end up having a prominent role in its low-temperature physical properties, as we show here. In particular magnons scatter the conduction electrons and have definite importance in the electrical resistivity of ferromagnetic metals. As we apply pressure

*mucio@cbpf.br

on $U_4Ru_7Ge_6$ and measure its resistivity, we have a rare opportunity to observe the evolution of the spin-wave stiffness of a ferromagnetic system as it approaches the QCP. Our transport measurements show a clear softening of the magnon modes as $U_4Ru_7Ge_6$ is driven to the putative ferromagnetic QCP (FQCP) with increasing pressure. In the present study, we obtain the quantum critical behavior of the stiffness of these excitations.

A similar program to accompany the quantum critical properties of antiferromagnetic metals as they are driven from the ordered magnetic phase to a magnetic QCP encounters several difficulties. First, these systems are, in general, anisotropic, with a (pressure-dependent) gap in the spin-wave spectrum. This prevents an unambiguous determination of the pressure-dependent spin stiffness from the electrical resistivity. The latter is expected to present an exponential temperature dependence due to the gap. This is, in fact, observed, confirming the importance of electron-magnon scattering [15,16] in these systems.

Recently, single-crystalline samples of $U_4Ru_7Ge_6$ were obtained [13,17]. They present a reorientation transition of the ferromagnetic moments with increasing temperature that has not been observed in polycrystalline samples [9–12]. The low residual resistivity of the single crystals [13] compared to polycrystalline ones shows that disorder is an important ingredient in the latter. However, as discussed below, the temperature dependence of the resistivity in the ferromagnetic phase is the same in single- and polycrystalline materials and can be attributed to electron-magnon scattering. Also the low-temperature specific heat of both types of crystals has a contribution due to magnons, as shown later.

Our work also concerns the important and actual problem of ferromagnetic quantum criticality in metals [18–22]. Experimental evidence and theoretical work show that in metallic ferromagnets, when driven to a FQCP either by external or chemical pressure, the magnetic transition may become discontinuous, and a FQCP cannot be attained [22]. However, there is also theoretical support and experimental results [22] showing that for sufficiently disordered ferromagnetic metals a FQCP can still exist, which justifies the interest in these systems. The present work agrees with these expectations [18,22] since it confirms the existence of a FQCP in our polycrystalline sample of $U_4Ru_7Ge_6$.

II. EXPERIMENT

The sample was prepared by arc melting of its high-purity metallic constituents in the ratio U:Ru:Ge = 1:2:2, under argon atmosphere, without further heat treatment. However, the x-ray diffractogram at room temperature showed a composition of $U_4Ru_7Ge_6$, with additional spurious phases [23], as discussed in detail below. The x-ray powder diffraction (XRD) at room temperature was performed using the Bruker AXS D8 Advance II diffractometer, with the LynxEye detector Cu source with K_α radiation.

The diffraction pattern was collected in a Bragg-Brentano configuration covering the angular range of $10°$ to $90°$, with incremental steps of $0.02°$. The XRD data were refined using the Rietveld method [14], implemented in the program FULL-PROF [24], available from the Institut Laue-Langevin [25]. The

profile function used to adjust the shape of the diffraction peaks was the pseudo-Voigt function.

Pressure-dependent resistivity measurements were carried out in a temperature range from 0.1 to 10 K in a noncommercial adiabatic demagnetization refrigerator. A standard 2.5-GPa piston cylinder type of cell was used, with a mixture of fluorinert FC70-FC77 as the pressure medium, pure lead as the pressure sensor at low temperatures, and manganin as a manometer for loading the cell at ambient temperature. We further performed measurements of electrical resistivity under magnetic fields up to 9 T and respective magnetoresistance measurements in the temperature range from 1.8 to 30 K in a commercial physical property measurement system (PPMS) DynaCool from Quantum Design at ambient pressure.

The specific heat measurements as a function of temperature were also performed in the PPMS DynaCool under different magnetic field values ranging from 0 to 7 T in the temperature interval from 2 to 15 K.

The magnetic characterization involved the application of external magnetic fields in dc and ac modes. The dc magnetization measurements were in the field-cooling (FC) mode in a field of 10 mT. For the ac susceptibility measurement, the parameters used were $H_{AC} = 1$ mT and $H_{DC} = 50$ mT at 3 kHz. Both types of measurements were performed from 2 to 300 K in the PPMS DynaCool (Quantum Design).

III. SAMPLE ANALYSIS

The XRD showed that the sample produced has a main phase of cubic crystalline structure of $U_4Ru_7Ge_6$ and secondary phases. After a detailed analysis of the diffraction pattern and identification of all peaks of minor intensities, it was found that the secondary phases could probably be Ru_2Ge_3 and γ-U. The Rietveld refinement of the x-ray diffractogram was performed first using the $U_4Ru_7Ge_6$ main compound phase. In the sequence, the Crystallographic Information File (CIF) data of the other phases were added in the base of the program; after adjustment, the presence of Ru_2Ge_3 and γ-U compounds was confirmed as secondary phases in the sample. The CIF data were obtained from the Inorganic Crystal Structure Database (ICSD).

Figure 1 shows the refinement of the XRD, where the black circles are the experimentally observed data, while the solid red line is the standard calculated by the refinement. The allowed Bragg positions are represented by vertical green bars, where each level corresponds to the peaks of the Bragg planes of each of the phases found. The planes (*hkl*) shown in Fig. 1 correspond to the peaks of the diffractogram of the predominant phase $U_4Ru_7Ge_6$, which appears in the amount of 78.08%. The parameters of the crystalline lattice and the amounts of each of the phases found as a result of the refinement, as well as their quality R factors, are described in Table I. The crystallographic data sheet ICSD 192067 [11] was used for the refinement of the phase $U_4Ru_7Ge_6$. In Table I, it is seen that the lattice parameters of all phases are in agreement with the literature [7,9,26,27]. The interatomic distance of the uranium atoms of the major phase $U_4Ru_7Ge_6$ is $d_{U-U} = 5.866$ Å, also agreeing with the literature [7,9].

An electron microprobe analysis of our sample was made using a scanning electron microscope (Jeol, model JSM-
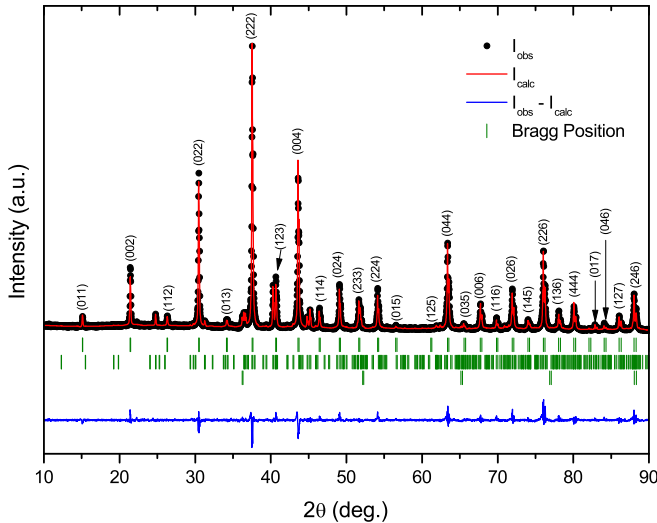
FIG. 1. Result of the Rietveld refinement of the x-ray diffraction pattern of the sample. The experimentally observed data are shown by the black circles, and the calculated standard is given by the solid red line. The allowed Bragg positions are represented by vertical green bars, where each level corresponds to each of the phases found: $U_4Ru_7Ge_6$ (78.06%), Ru_2Ge_3 (20.78%), and γ-U (1.16%). The difference pattern ($I_{obs} - I_{calc}$) is represented by the solid blue line. The planes (hkl) shown are of the major phase $U_4Ru_7Ge_6$.

7100F), with energy dispersive spectroscopy. It clearly shows three distinct phases, with proportions similar to those obtained by x-ray diffraction. The Ru_2Ge_3 and γ-U are seen as phases segregated from the main $U_4Ru_7Ge_6$ phase that, in turn, pervades through the bulk material [28].

While uranium in its allotropic forms has a higher resistivity than copper [29], it has a weak paramagnetic behavior, exhibiting paramagnetism almost independent of temperature [30,31]; the second spurious phase of the sample, Ru_2Ge_3, is a semiconductor and strongly diamagnetic, exhibiting a paramagnetic contribution above 900 K due to the structural transition [32], from orthorhombic (center symmetric) to tetragonal (nonsymmetrical) [33]. Thus, in this work, we state that the low-temperature magnetic, thermodynamic, and

TABLE I. Crystallographic parameters obtained from the Rietveld refinement of the sample. The quality of the refinement is $R_p = 19.3\%$, $R_{wp} = 16.9\%$, $R_{exp} = 8.98\%$, $\chi^2 = 3.537$, $S = 1.881$.

	Phase		
	$U_4Ru_7Ge_6$	Ru_2Ge_3	γ-U
Composition	78.06%	20.78 %	1.16%
Crystalline structure	cubic	orthorhombic	cubic
Space group	$Im\bar{3}$	$Pbcn$	$Im\bar{3}m$
Data sheet CIF-ICSD[a]	192067	85205	44392
Lattice parameters			
a (Å)	8.295813	11.436	3.504737
b (Å)		9.238	
c (Å)		5.716	

[a]Crystallographic information file, Inorganic Crystal Structure Database.
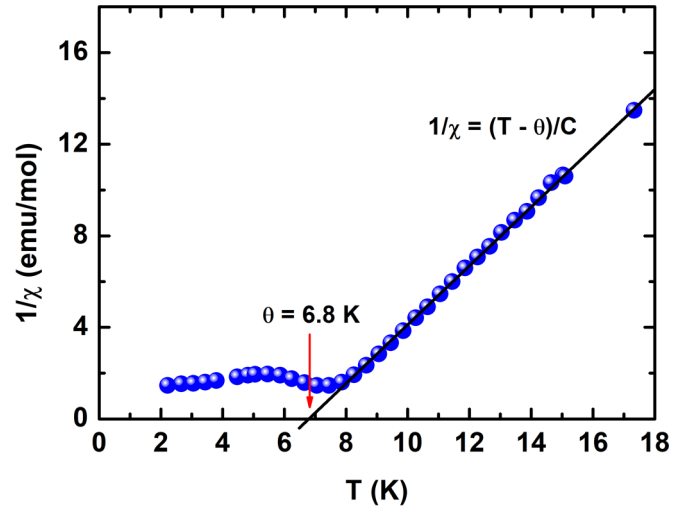
FIG. 2. The inverse of the magnetic ac susceptibility $\chi_{AC}(T)$ of the sample as a function of temperature for a frequency of 3 kHz, an ac field of 1 mT, and a dc field $H_{DC} = 50$ mT. The arrow marks the Curie-Weiss temperature that is very close to the ferromagnetic transition of $U_4Ru_7Ge_6$, indicated by the peak in the susceptibility.

transport properties of our sample are due to the main phase $U_4Ru_7Ge_6$ with negligible contribution from the secondary phases.

IV. MAGNETIC PROPERTIES AND EVIDENCE FOR SPIN WAVES

The inverse of the magnetic ac susceptibility $\chi_{AC}(T)$ of our sample as a function of temperature is shown in Fig. 2 from 2 to 18 K. The data show a peak at $T_C = 6.8$ K that we identify as the Curie temperature, below which $U_4Ru_7Ge_6$ becomes ferromagnetic. This coincides with the T_C found in Ref. [7] ($T_C = 6.8$ K) but is smaller than those found in Refs. [9,12] that range in the interval between 10.0 and 13.0 K. Above T_C the susceptibility follows a Curie-Weiss law from which we extract an effective magnetic moment of $\approx 2.14\mu_B$ per uranium atom [34]. This is large compared to the value obtained from the saturation magnetization in large magnetic fields ($0.2\mu_B$ per uranium atom) [7,13] but smaller than the value of $2.54\mu_B$ extracted from the Curie-Weiss behavior of the susceptibility at high temperatures (300 K $\lesssim T \lesssim$ 500 K) [9]. It is interesting that the Curie-Weiss temperature θ indicated by an arrow in Fig. 2 is very close to the ferromagnetic critical temperature T_C obtained from the peak in χ_{AC}. This mean-field behavior is consistent with the rather large uranium moment in a cubic structure and indicates that ferromagnetic fluctuations are important only close to T_C.

In ferromagnetic systems, metallic or insulating, below T_C the low-temperature magnetic elementary excitations are long-wavelength spin waves with the dispersion relation $\hbar\omega_k = \Delta + Dk^2$. The gap Δ may be due to the magnetocrystalline anisotropy, dipolar interactions, or the Zeeman energy if an external magnetic field H_a is applied to the material. The quantity D is the *spin-wave stiffness* of the magnetic system. For a soft ferromagnet with negligible anisotropy, in zero field and in the temperature range of our experiments,
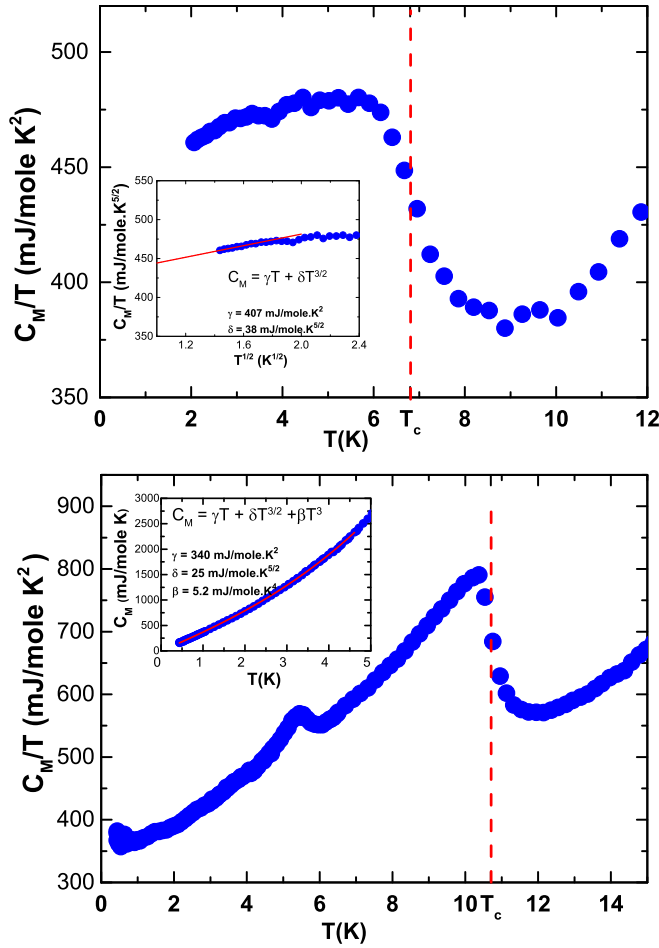
FIG. 3. Molar specific heat plotted as C_M/T versus T for our sample (top panel) and that of Ref. [13] (bottom panel). The Curie temperatures T_c obtained from magnetic and transport properties are also shown. The insets show the contribution of magnons to the specific heat. In the former case this is best shown plotting C_M/T versus $\sqrt{T}$ and fitting with a straight line. In the latter due to an important phonon (T^3), even at the lowest temperatures, this is shown fitting a plot of C_M versus T.

the gap, in general, can be neglected, and the spectrum is purely quadratic in the wave vector k. Notice that in this case, the mode $\omega_{k=0} = 0$ is the Goldstone mode of the rotationally invariant system [5].

Figure 3 (top panel) shows the low-temperature behavior of C_M/T, the molar specific heat divided by temperature, of our sample of polycrystalline $U_4Ru_7Ge_6$. We considered that only 78% of the total molecular weight is due to the main phase. We also show (bottom panel) the single-crystal data of Ref. [13] plotted in the same way. Notice that in both cases the Curie temperatures T_c obtained by magnetic or transport measurements are associated with inflection points in the C_M/T versus T plots. The insets show a $T^{3/2}$ contribution for the specific heat due to gapless ferromagnetic magnons with a quadratic dispersion. In the case of our sample this is best shown by plotting C_M/T versus $\sqrt{T}$ and fitting with a straight line. For the single-crystal data, due to an important phonon T^3 contribution even at the lowest temperatures this is best accomplished by directly fitting C_M versus T. Notice

that the coefficient of the spin-wave contribution obtained for the polycrystal $\delta = 0.038$ J/mol $K^{5/2}$ is of the same order as that in the single crystal of $U_4Ru_7Ge_6$, $\delta = 0.025$ J/mol $K^{5/2}$. However, the larger value of the former indicates that the magnons are softer in the polycrystalline material [see Eq. (1) below]. An analysis of the resistivity data (discussed below) also leads us to conclude that the general effect of disorder in this sample when compared with the single crystal is to soften the magnetic excitations in the former.

The large linear temperature-dependent terms found in the specific heat of both samples are due to the heavy quasiparticles of the metallic $U_4Ru_7Ge_6$ compound [13]. In our sample, the coefficient of this term, $\gamma = 407$ mJ/mol K^2 (or $\gamma_0 = 102$ mJ/mol U K^2), is similar to that given in the literature for polycrystalline materials [7,12,13].

A phonon contribution to the specific heat of our sample also becomes apparent in a plot of C_M/T versus T^2, where linear behavior is observed in the temperature interval from ≈ 15 to 30 K. The Debye temperature obtained from the inclination of this line is $\Theta_D = 276$ K [7]. The data show that the phonon contribution in this case can be safely neglected in the temperature region below T_C.

Unfortunately, the magnetization data of the $U_4Ru_7Ge_6$ single crystal are hard to analyze due to the reorientation transition of the magnetization in the ordered ferromagnetic phase [13].

In spin-wave theory, for a cubic ferromagnetic system with gapless magnon excitations, the expression for the contribution of these modes to the low-temperature specific heat per unit volume is calculated as [35]

$$C_V = \frac{1}{V}\left(\frac{\partial E}{\partial T}\right)_V = \frac{15}{4}\zeta\left(\frac{5}{2}\right)\left(\frac{1}{4\pi D}\right)^{3/2} k_B^{5/2} T^{3/2}. \quad (1)$$

This expression allows us to obtain the spin-wave stiffness D from the coefficient of the $T^{3/2}$ term of the specific heat in the experimental data, as shown in Fig. 3. Notice that $C_M = C_V \mathcal{V}_M$, with C_V given by Eq. (1) and $\mathcal{V}_M$ being the molar volume. We get, using the value of δ above, $D = 32 \pm 1$ meV Å^2. The error here is mainly due to uncertainty in the volume of the sample.

Figure 4 shows the normalized low-temperature magnetization of $U_4Ru_7Ge_6$ as a function of $T^{3/2}$. The linear behavior of the magnetization in this plot implies that at low temperatures it decreases according to Bloch's $T^{3/2}$ law. This is a clear signature that this decrease is due to the thermal excitation of ferromagnetic magnons [35]. Bloch's law yields

$$M(T)/M(0) = 1 - BT^{3/2} \quad (2)$$

at low temperatures [35]. The coefficient B is related to the spin-wave stiffness by [35]

$$B = \frac{\zeta(3/2)g\mu_B}{M(0)}\left(\frac{k_B}{4\pi D}\right)^{3/2}. \quad (3)$$

Using the experimental value of B obtained from Fig. 4 in Eq. (3), we find $D = 27 \pm 1$ meV Å^2, where the error comes from the uncertainty in the volume of the sample. In Eq. 2, $M(0) = 6.1 \times 10^6$ emu/m^3.

The values for the spin-wave stiffness obtained above from the low-temperature specific heat and magnetization
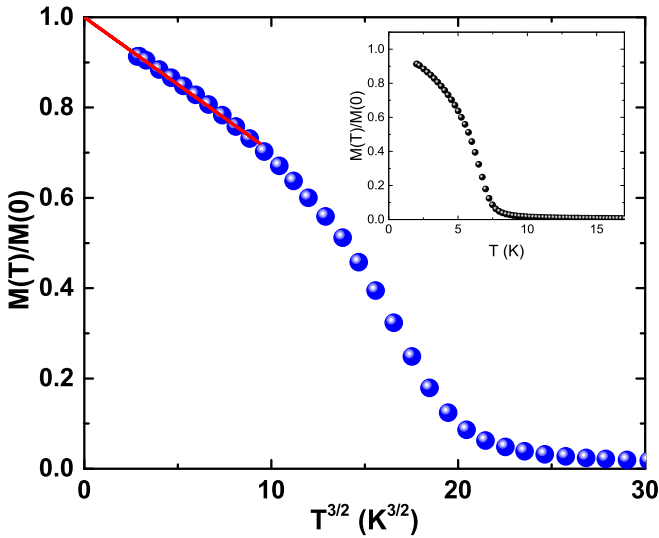
FIG. 4. Normalized low-temperature magnetization of the ferromagnet $U_4Ru_7Ge_6$ versus $T^{3/2}$ measured in 10 mT field-cooling. At low temperatures, the magnetization decreases with a Bloch $T^{3/2}$ law. We get for the coefficient in Eq. (2) $B = 0.030$ K$^{-3/2}$. In the inset a plot of $M(T)/M(0)$ versus temperature shows the sharpness of the transition.

measurements, $D = 32 \pm 1.0$ meV Å^2 and $D = 27 \pm 1.0$ meV Å^2, respectively, are consistent and of the expected order of magnitude for a soft metallic ferromagnet with a Curie temperature of $T_C \approx 10$ K. For example, in ferromagnetic Ni with $T_C \approx 631$ K [35] the experimentally obtained spin-wave stiffness ranges from $D \approx 422$ meV Å^2 to $D \approx 555$ meV Å^2 [36] when extracted from Bloch's law and measured directly by neutron scattering, respectively. These results strongly support the idea that ferromagnetic magnons play an important role in the thermodynamic properties of the cubic ferromagnetic $U_4Ru_7Ge_6$ below its Curie temperature.

V. TRANSPORT PROPERTIES

In ferromagnetic metals, the scattering of conduction electrons by ferromagnetic spin waves gives rise to a T^2 temperature-dependent contribution to the electrical resistivity of these materials [37]. This T^2 term has, indeed, been found in a previous study of $U_4Ru_7Ge_6$ [12], but it has been attributed to electron-electron scattering as in strongly correlated paramagnetic metals. However, in a long-range-ordered ferromagnetic metal, with polarized bands and gapless spin-wave modes, the main scattering is due to these elementary excitations. In fact, this is the main form that electron-electron scattering assumes in an itinerant ferromagnetic metal. Here, we give evidence that in ferromagnetic $U_4Ru_7Ge_6$ a substantial part of the T^2 term in its resistivity is due to electron-magnon scattering. This contribution to the resistivity is given by [37]

$$\rho = AT^2 = \frac{32}{3}\zeta(2)\pi^2\tilde{\rho}_a\left(\frac{\Delta E}{E_F}\right)\left(\frac{k_BT}{Dk_F^2}\right)^2, \quad (4)$$

where $\tilde{\rho}_a$ is a constant with units of resistivity and k_F and E_F are the Fermi wave vector and Fermi energy of the f electrons, respectively. The quantity $(\Delta E/E_F) = 2q_{max}/k_F$, where q_{max} is the maximum wave vector for which the quadratic spin-wave dispersion relation, $\hbar\omega = Dk^2$, holds. The spin-wave stiffness appears in the denominator of this equation, such that the softer the magnon modes are, the larger this contribution to the resistivity is. At a FQCP, where the spin-wave stiffness vanishes, the resistivity of the metal is given by [37]

$$\rho = 64\pi\tilde{\rho}_a\Gamma\left(\frac{8}{3}\right)\zeta\left(\frac{5}{3}\right)\left(\frac{3\pi k_BT}{E_F}\right)^{5/3}. \quad (5)$$

In the next section, we will present results for the electrical resistivity of our sample as a function of temperature for different applied pressures and magnetic fields. As pressure increases, the ferromagnetic Curie temperature vanishes smoothly at a FQCP at a critical pressure, $P_c = 1.7 \pm 0.02$ GPa. The resistivity curves we obtain present no hysteresis for any pressure. We find no evidence of a behavior that could indicate a first-order transition as the Curie temperature of the sample is reduced and made to vanish. As we accompany the variation of the coefficient of the T^2 term with increasing pressure, we observe a smooth increase in this coefficient that we attribute entirely, according to Eq. (4), to a decrease in the spin-wave stiffness as the FQCP is approached. At the critical pressure the resistivity follows a $T^{5/3}$ behavior in agreement with Eq. (5).

We have verified that the electrical resistivity of the single-crystalline sample of Ref. [13] (ambient pressure, zero magnetic field) can also be described by $\rho = \rho_0 + AT^2$ in the ferromagnetic phase. This transport property is insensitive to the rearrangement of the moments. Although the residual resistivity of the single crystal ($\rho_0 = 41$ $\mu\Omega$/cm) is much smaller than that of the polycrystal ($\rho_0 = 240$ $\mu\Omega$/cm) under the same conditions, the coefficient of the T^2 term ($A = 0.39$ $\mu\Omega$/cm K^2) of the former is smaller than that of the disordered sample ($A = 0.68$ $\mu\Omega$/cm K^2). The observed larger value of the coefficient A in our sample, together with Eq. (4), shows that the magnons are softer in the disordered material.

Pressure experiments

Figure 5 shows the low-temperature behavior of the electrical resistivity of $U_4Ru_7Ge_6$ as a function of pressure. All pressure experiments were carried out in zero external magnetic field. The electrical resistivity behaves smoothly, with no detectable hysteresis for all pressures of the experiments.

At very low temperatures, it presents a T^2 dependence, both above and below the critical pressure $P_c \approx 1.7$ GPa, and is well described by $\rho = \rho_0 + A(P)T^2$. The exception is for pressures very close to P_c, where $\rho(T) \propto T^{5/3}$, as shown in Fig. 6. This is the expected power law behavior for a ferromagnetic metallic system close to a FQCP [see Eq. (5)].

In Fig. 7, we show physical parameters obtained from the resistivity data as a function of pressure.

(i) In principle, the observation of a clear-cut bend (or kink) in the T dependence of the electrical resistivity is an indication of the onset of magnetic ordering (see Fig. 5). The precise determination of T_C is obtained from the second derivative of
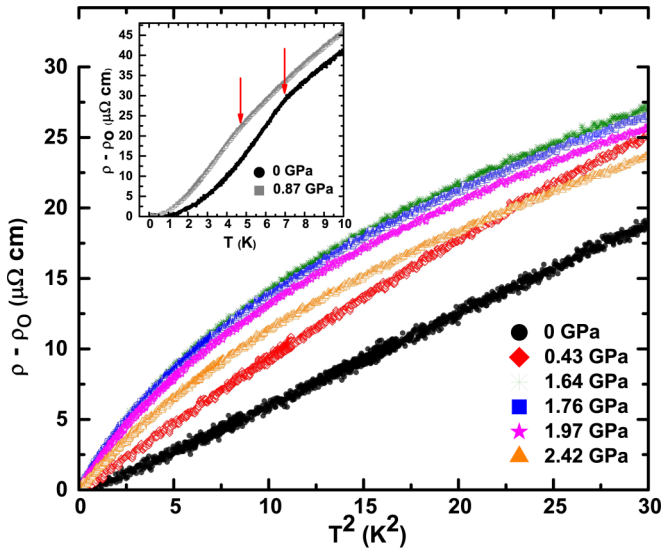
FIG. 5. Resistivity of the ferromagnet $U_4Ru_7Ge_6$ versus the square of temperature for different applied pressures above and below the critical pressure. The residual resistivity and the coefficients of the low temperature T^2 terms for different pressures are shown in Fig. 7. The inset shows the resistivity versus temperature for selected pressures, with arrows showing the magnetic transitions.

the smoothed electrical resistivity data [38]. In Fig. 7(a), we plot the T_C obtained in this way and draw through these points a curve from a fit using the expected power law behavior for an itinerant FQCP, $T_C \propto |P_c - P|^\psi$, where the *shift* exponent [5] $\psi = z/(d + z - 2) = 3/4$ since the dynamic exponent is $z = 3$ in this case [5]. The curve gives a reasonable description of the pressure-dependent Curie temperatures.

(ii) Figure 7(b) shows the pressure dependence of the residual resistivity. This is nearly constant in the ferromagnetic phase, with a small drop close to the critical pressure.
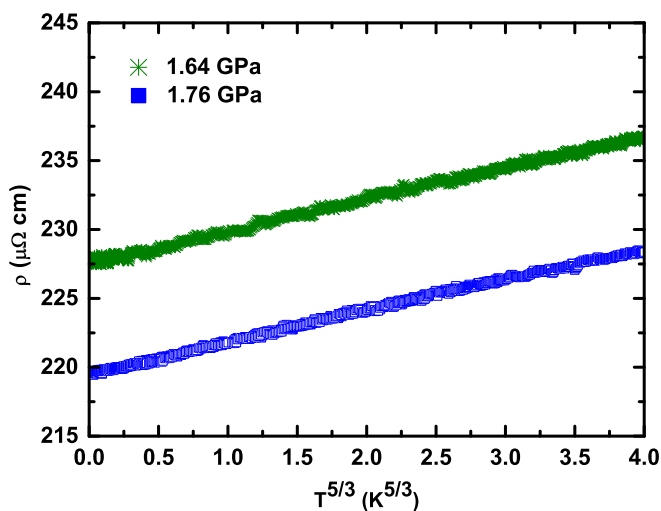
FIG. 6. Low-temperature resistivity of the ferromagnet $U_4Ru_7Ge_6$ for pressures very close to the pressure where ferromagnetism is suppressed. The plot shows the $T^{5/3}$ power law behavior expected for an itinerant $3d$ ferromagnet at a FQCP [see Eq. (5)].
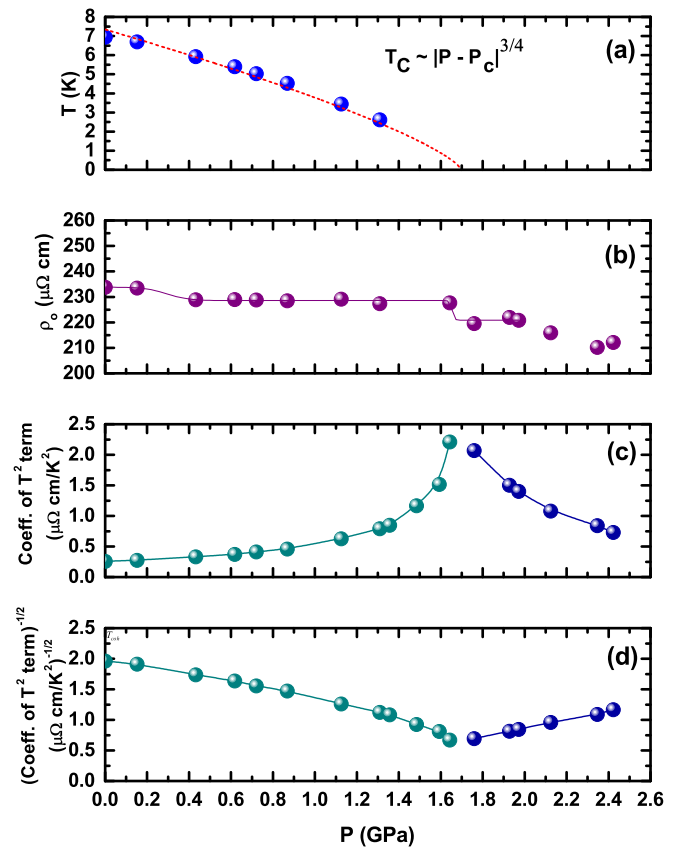
FIG. 7. Parameters extracted from the temperature-dependent resistivity curves for different pressures. (a) The Curie temperature obtained from the second derivative of the resistivity (see text). The dashed line corresponds to a fitting with the expression $T_C \propto |P_c - P|^\psi$, with $\psi = 3/4 = 0.75$, the expected shift exponent for a $3d$ itinerant ferromagnet (see text), and $P_c = 1.7$ GPa. (b) The residual resistivity as a function of pressure. The coefficients of the T^2 term in the resistivity (c) above and (d) below P_c.

(iii) Figures 7(c) and 7(d) refer to the pressure dependence of the coefficients of the T^2 term of the resistivity. These coefficients rise on both sides of the phase diagram as the critical pressure is approached from below and above in a nonsymmetric fashion. In the paramagnetic phase, above P_c, this term is due to scattering by paramagnons, and its coefficient is proportional to the square of the inverse of the coherence temperature [39], $T_{coh} \propto |P - P_c|^{\nu z}$, with $\nu z = 3/2$ for a three-dimensional itinerant ferromagnetic system [39]. As can be seen in Figs. 7(c) and 7(d), we do not have enough data for T_{coh} close to the critical pressure to be able to determine its power law dependence on the distance from criticality. Sufficiently far from P_c, T_{coh} depends linearly on this distance, which suggests local quantum critical behavior [5].

(iv) For pressures below P_c, in the ferromagnetic phase, according to Eq. (4), the coefficient of the T^2 term in the resistivity is related to spin-wave stiffness D, $A(P) \propto 1/D^2$. In itinerant $3d$ ferromagnets, the coupling of the order parameter to particle-hole excitations gives rise to nonanalytic behavior of the spin-wave stiffness as a function of the magnetization m [18,40]. For a disordered quantum itinerant $3d$ ferromagnet,

$$D(m \to 0) = c_3 m[m^{-1/2} + O(1)], \qquad (6)$$
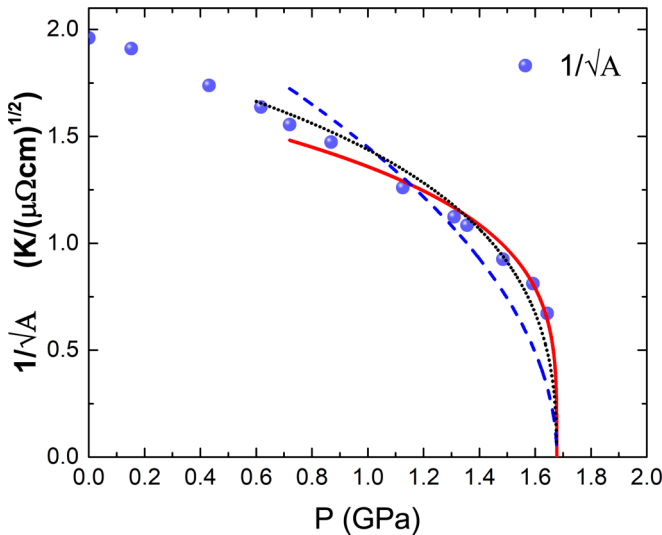
FIG. 8. Pressure dependence of the quantity $1/\sqrt{A}$, which mimics that of the spin-wave stiffness D. The dashed line is the mean-field prediction $D \propto m$, while the solid and dotted lines are best fits using Eqs. (6) and (7), respectively. In every case $P_c = 1.64$ GPa.

while for the clean system,

$$D(m \to 0) = \tilde{c}_3 m[\ln(1/m) + O(1)], \qquad (7)$$

where c_3 and $\tilde{c}_3$ are positive constants [40]. In a 3d quantum metallic ferromagnet the magnetization vanishes close to the FQCP as $m \propto |P_c - P|^\beta$ with a mean-field exponent $\beta = 1/2$ [41]. In Fig. 8 we plot the pressure dependence of the quantity $1/\sqrt{A}$ that mimics that of the spin-wave stiffness for pressures approaching the FQCP. We can compare in Fig. 8 the fitting using the simple mean-field expression $D \propto m \propto \sqrt{(P_c - P)}$ and those using Eqs. (6) and (7). The quality of the fittings with these expressions, for the disordered and clean ferromagnets, respectively, is similar. They clearly give a better description of the data than the simple mean field. On the other hand, the validity of Eq. (7) in the ordered phase of the clean ferromagnet would imply a discontinuous vanishing of this ordering with pressure [18,40], for which we find no evidence. We are left then with Eq. (6) describing the correct quantum critical behavior of the spin-wave stiffness, in agreement with the disordered nature of our sample.

VI. EFFECT OF AN EXTERNAL MAGNETIC FIELD

In this section, we study the effect of an applied magnetic field on the thermodynamic and transport properties of our sample at ambient pressure. In ferromagnets, a magnetic field is the conjugate of the order parameter and destroys the thermodynamic phase transition. This is different from the antiferromagnet where a uniform magnetic field just shifts the transition. The low-temperature magnetic excitations of the ferromagnet in an external magnetic field are still magnons, but they become partially quenched by a *Zeeman gap* due to the coupling of the magnetic moments to the field.

This reduces the influence and contribution of spin waves to the low-temperature properties, i.e., for $k_B T < \Delta$, where Δ is the Zeeman gap.
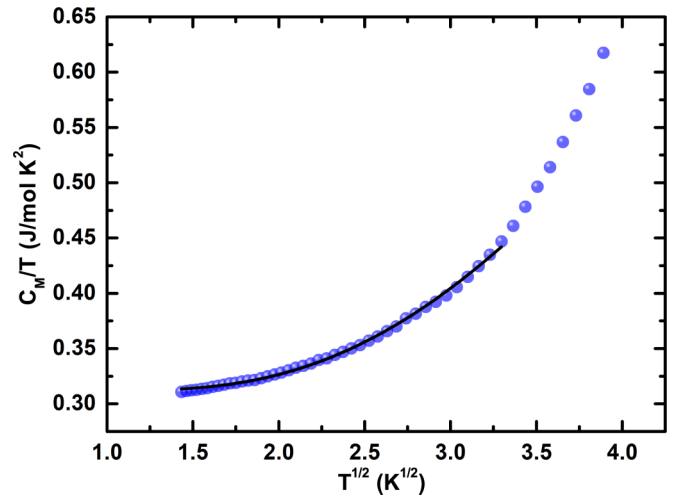
FIG. 9. Specific heat of $U_4Ru_7Ge_6$ as a function of temperature in an external magnetic field $H_a = 7$ T. The fitting curve $C_M/T = \gamma + b\sqrt{T}e^{-\Delta/T}$ includes an exponential term that accounts for the *freezing* of the magnons by the external field. The parameters $\gamma = 310$ mJ/mol K^2 and $\Delta = 9.1$ K.

In Fig. 9 we show the specific heat as a function of temperature in an applied field of 7 T. The low-temperature specific heat is well fitted by the expression $C_M/T = \gamma + b\sqrt{T} \exp(-\Delta/T)$. The exponential term takes into account the quenching of the magnons by the Zeeman gap $\Delta = (g\mu_B S H_a)/k_B$, expressed here in temperature scale. From this fit we can determine the coefficient of the linear term $\gamma(H_a)$ and the Zeeman gap $\Delta(H_a)$ for several values of the external magnetic field, as shown in Figs. 10 and 11, respectively. Figure 10 shows that the coefficient of the linear term in the specific heat is reduced as the external field is applied. The simplest interpretation for this effect is that the Zeeman splitting of the polarized bands causes a decrease in the density of states at the Fermi level [42]. This behavior of $\gamma(H_a)$ is quite distinct from that in antiferromagnet heavy
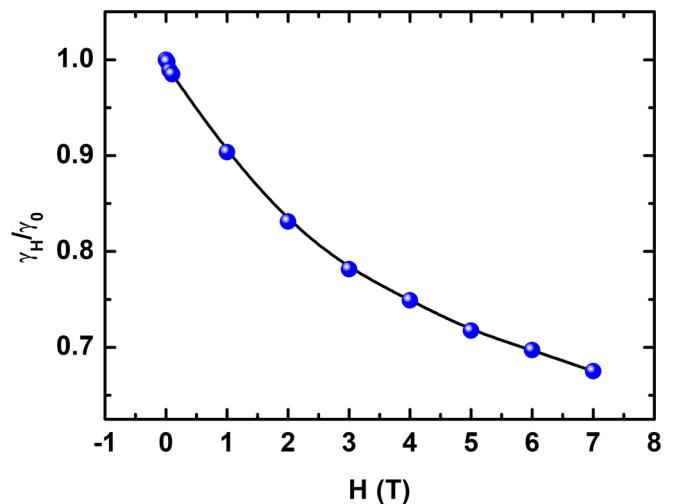
FIG. 10. The coefficient of the linear term in the specific heat as a function of the external magnetic field. The line is a guide to the eyes.
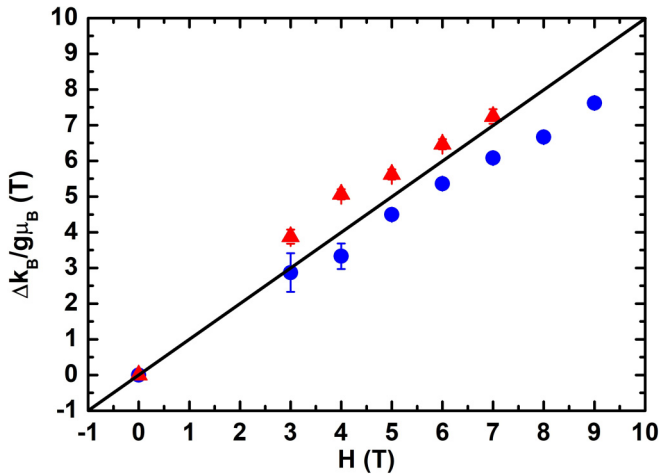
FIG. 11. The spin-wave gaps extracted from the specific heat data (triangles) and from the resistivity (circles) using the expressions in the text. The straight line is the result expected from the simplest spin-wave theory (see text).

fermions [43], as expected from the different roles of H_a in these systems.

The suppression of the magnons by the magnetic field also decreases the low-temperature electrical resistivity due to a partial freezing of the electron-magnon scattering. The low-temperature electrical resistivity shown in Fig. 12 for $H_a = 7$ T is well described by the expression [44]

$$\rho = \rho_0 + a\Delta T e^{-\Delta/T}\left(1 + 2\frac{T}{\Delta}\right). \tag{8}$$

The gap Δ (in units of temperature) extracted from the resistivity data for several values of the applied magnetic field
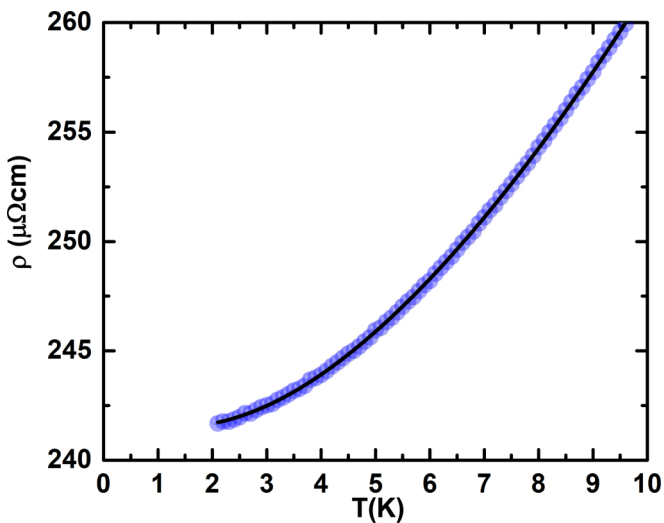
FIG. 12. Resistivity of our sample as a function of temperature in an external magnetic field $H_a = 7$ T. The fitting curve $\rho = \rho_0 + b_r T^2 e^{-\Delta/T} + c_r T e^{-\Delta/T}$ (black) takes into account the quenching of the magnons by the magnetic field that suppresses the electron-magnon scattering at very low temperatures (see text). The gap for this field is $\Delta = 6.5$ K.
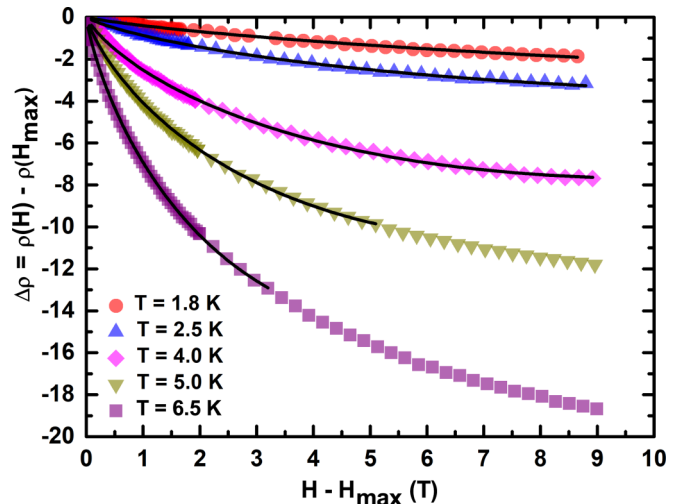
FIG. 13. Magnetoresistance of our sample as a function of magnetic field for several fixed temperatures. The lines are two-parameter fittings (*a* and *b*) using the expression $\Delta\rho = a(H - H_{max})\ln(H - H_{max})/b$ as given in the text [46].

is shown in Fig. 11. The gaps obtained from the transport and thermodynamic data are in satisfactory agreement. The straight line in this plot shows the expected value for the Zeeman gap in the simplest (non-self-consistent) spin-wave theory [45].

For completeness, we now present magnetoresistance results at ambient pressure for our sample. Resistivity is measured as a function of magnetic field for fixed temperatures below the Curie temperature. For small fields, $H_a \ll 1$ T, and very low temperatures, the magnetoresistance is positive and reaches a maximum at H_{max} and then decreases almost linearly with field for $H_a > H_{max}$. Magnetoresistance of multiband ferromagnetic metals, like transition metals, has been intensively studied both experimentally and theoretically [46]. Raquet *et al.* [46] have shown that for systems with a light *c* band of conduction electrons and a heavy *f* band of quasi-particles, intraband scattering in the conduction *c* band can be neglected. Notice that due to the strong *c*-*f* hybridization in $U_4Ru_7Ge_6$ [13,14] the bands have a hybrid character, and those referred to above are, in fact, bands with *mostly c band* and *mostly f band* characters. Considering electron-magnon scattering, which involves an intraband *f*-*f* and interband *c*-*f* spin-flip process, Raquet *et al.* [46] showed that in the presence of a magnetic field, the magnetoresistance roughly follows a $H_a \ln H_a$ dependence for temperatures above approximately $T_C/5$. In Fig. 13 we plot the magnetoresistance, defined as $\Delta\rho = \rho(H_a, T) - \rho(H_{max}, T)$ as a function of $H_a - H_{max}$, for different fixed temperatures. H_{max} is the value of the magnetic field for which the magnetoresistance reaches a maximum before it starts to decrease. We attribute the positive magnetoresistance at low fields and low temperatures to the existence of domain walls that are eventually removed at H_{max}. Figure 13 also shows the fittings using the simple logarithmic law obtained in Ref. [46], $\Delta\rho = a\delta H \ln(\delta H/b)$, with $\delta H = H - H_{max}$. This law gives a good description of our data.

VII. CONCLUSIONS

The study of systems close to quantum criticality is an exciting area of research. In the case of itinerant ferromagnets driven to a magnetic instability, there is theoretical and experimental evidence that quantum critical behavior is avoided and a first-order transition occurs before the FQCP is reached [18,22,47]. In this work we present a thorough investigation of the ferromagnetic heavy-fermion system $U_4Ru_7Ge_6$ as it is driven to the paramagnetic state under applied pressure. The results of the transport properties under pressure show no sign of a discontinuous behavior as T_C is reduced. The resistivity curves present no hysteresis effects for any pressure before or after ferromagnetism is suppressed. Disorder is certainly present in our system, as evidenced by its high residual resistivity. It is possible that it is responsible for the observed continuous quantum critical behavior. We have shown that the behavior of the spin-wave stiffness close to quantum criticality is consistent with that expected for a disordered ferromagnet. Whenever possible, we compared our results with those obtained at ambient pressure in a single-crystalline sample of $U_4Ru_7Ge_6$ [13]. This shows that one of the effects of disorder is to soften the magnetic excitations in the ferromagnetic phase of the polycrystal compared to those of the single crystal. It would be very interesting to perform a study similar to that presented here in single crystals of $U_4Ru_7Ge_6$.

Although disorder is present in our sample, it is not sufficiently strong to give rise to localization effects or Griffith's singularities. On the contrary, we have shown that it shows many of the properties expected for an itinerant clean system, such as the $T^{5/3}$ temperature dependence of the resistivity at its FQCP.

$U_4Ru_7Ge_6$ is a unique uranium compound with negligible anisotropy. This implies that spin waves, the elementary excitations of a ferromagnetic metal, can be easily excited and play a fundamental role in the thermodynamic and transport properties of this system at low temperatures. We have shown that, as the FQCP is approached with increasing pressure, the spin-wave stiffness softens and we obtain its quantum critical behavior. In our polycrystal material this is consistent with that expected for a disordered itinerant ferromagnet [22]. Inelastic neutron scattering experiments could be performed to measure directly the spin-wave stiffness of $U_4Ru_7Ge_6$. This could be compared with the values obtained in the present study using thermodynamic experiments. Especially interesting would be to observe with neutrons the softening of the magnons with increasing pressure.

In summary our results on the ferromagnetic $U_4Ru_7Ge_6$ provide strong evidence for the existence of a pressure-induced ferromagnetic-paramagnetic quantum phase transition in this system that is accompanied by a softening of the elementary excitations of the ordered phase. Although disorder certainly plays a role in our system, its quantum critical behavior shows features expected for a clean, itinerant FQCP.

[1] *Strongly Correlated Electron Systems: Reports on the Progress of the Field*, edited by L. H. Green, J. Thompson, and J. Schmallian, special issue of Rep Prog. Phys. **80**(3) (2017); Y. Chen, Z. Weng, S. Michael, X. Lu, and H. Yuan, Chin. Phys. B **25**, 077401 (2016).

[2] D. Aoki and J. Flouquet, J. Phys. Soc. Jpn. **81**, 011003 (2012).

[3] P. F. S. Rosa, Y. Luo, E. D. Bauer, J. D. Thompson, P. G. Pagliuso, and Z. Fisk, Phys. Rev. B **92**, 104425 (2015).

[4] C. Adriano, P. F. S. Rosa, C. B. R. Jesus, T. Grant, Z. Fisk, D. J. Garcia, and P. G. Pagliuso, J. Appl. Phys. **117**, 17C103 (2015).

[5] M. A. Continentino, *Quantum Scaling in Many-Body Systems: An Approach to Quantum Phase Transitions* (Cambridge University Press, Cambridge, 2017).

[6] L. G. Akselrud, J. P. Jarmoljuk, and E. I. Gladyshevskij, Dopov. Akad. Nauk **4**, 359 (1978).

[7] S. A. M. Mentink, G. J. Nieuwenhuys, A. A. Menovsky, and J. A. Mydosh, J. Appl. Phys. **69**, 5484 (1991).

[8] H. H. Hill, *Plutonium 1970 and Other Actinides*, edited by W. N. Miner (American Institute of Mining, Metallurgical, and Petroleum Engineers, New York, 1970), p. 2.

[9] B. Lloret, B. Buffat, B. Chevalier, and J. Etourneau, J. Magn. Magn. Mater. **67**, 232 (1987).

[10] E. Colineau, F. Wastin, E. J. Higgins, and J. Rebizant, J. Alloys Compd. **317**, 336 (2001).

[11] S. F. Matar, B. Chevalier, and R. Pöttgen, Solid State Sci. **27**, 5 (2014).

[12] H. Hidaka, S. Takahashi, Y. Shimizu, T. Yanagisawa, and H. Amitsuka, J. Phys. Soc. Jpn. **80**, SA102 (2011).

[13] M. Vališka, M. Diviš, and V. Sechovsky, Phys. Rev. B **95**, 085142 (2017).

[14] H. M. Rietveld, J. Appl. Crystallogr. **2**, 65 (1969).

[15] M. A. Continentino, S. N. de Medeiros, M. T. D. Orlando, M. B. Fontes, and E. M. Baggio-Saitovitch, Phys. Rev. B **64**, 012404 (2001).

[16] S. N. de Medeiros, M. A. Continentino, M. T. D. Orlando, M. B. Fontes, E. M. Baggio-Saitovitch, A. Rosch, and A. Eichler, Physica B (Amsterdam, Neth.) **281–282**, 340 (2000).

[17] M. Vališka, M. Klicpera, P. Doležal, O. Fabelo, A. Stunault, M. Diviš, and V. Sechovský, Phys. Rev. B **97**, 125128 (2018).

[18] T. R. Kirkpatrick and D. Belitz, Phys. Rev. B **85**, 134451 (2012).

[19] J. Pospíšil, P. Opletal, M. Valiska, Y. Tokunaga, A. Stunault, Y. Haga, N. Tateiwa, B. Gillon, F. Honda, T. Yamamura, V. Niznansky, E. Yamamoto, and D. Aoki, J. Phys. Soc. Jpn. **85**, 034710 (2016).

[20] T. R. Kirkpatrick and D. Belitz, Phys. Rev. Lett. **115**, 020402 (2015).

[21] P. Opletal, J. Prokleska, J. Valenta, P. Proschek, V. Tkac, R. Tarasenko, M. Behounkova, S. Matouskova, M. M. Abd-Elmeguid, and V. Sechovský, npj Quantum Mater. **2**, 29 (2017).

[22] M. Brando, D. Belitz, F. M. Grosche, and T. R. Kirkpatrick, Rev. Mod. Phys. **88**, 25006 (2016).

[23] For details on sample preparation see N. T. Huy, Y. K. Huang, and A. de Visser, J. Magn. Magn. Mater. **321**, 2691 (2009); J. Pospíšil, K. Prokes, M. Reehuis, M. Tovar, J. P. Vejpravova, J. Prokleska, and V. Sechovsky, J. Phys. Soc. Jpn. **80**, 084709 (2011).

[24] J. Rodríguez-Carvajal, Physica B (Amsterdam, Neth.) **192**, 55 (1993); T. Roisnel and J. Rodríguez-Carvajal, Mater. Sci. Forum **378–381**, 118 (2001).

[25] I. Laue-Langevin, FULLPROF, https://www.ill.eu/sites/fullprof/.

[26] D. J. Poutcharovsky and E. Parthe, Acta Crystallogr., Sect. B **30**, 2692 (1974).

[27] I. Grenthe, J. Drozdzynski, T. Fujino, E. C. Buck, T. E. Albrecht-Schmitt, and S. F. Wolf, in *The Chemistry of the Actinide and Transactinide Elements*, 3rd ed., edited by L. R. Morss, N. M. Edelstein, and J. Fuger (Springer, Dordrecht, 2008), Vol. 1, pp. 253–698.

[28] M. P. Nascimento, Ph.D. thesis, Centro Brasileiro de Pesquisas Físicas, 2018.

[29] S. Arajs, R. H. Flora, and E. E. Anderson, J. Nucl. Mater. **37**, 89 (1970).

[30] L. F. Bates and D. Hughes, Proc. Phys. Soc. B **67**, 28 (1954).

[31] C. J. Kriessman, Jr., and T. R. McGuire, Phys. Rev. **85**, 71 (1952).

[32] C. P. Susz, J. Muller, and E. Parthe, J. Less-Common Met. **71**, 1 (1980).

[33] D. J. Poutcharovsky, K. Yvon, and E. Parthe, J. Less-Common Met. **40**, 139 (1975).

[34] S. Blundell, in *Magnetism in Condensed Matter* (Oxford University Press, Cambridge, 2001), pp. 195–196.

[35] F. Keffer, in *Encyclopedia of Physics* (Springer, Berlin, 1966), Vol. 18(2), pp. 1–273.

[36] M. Pajda, J. Kudrnovsky, I. Turek, V. Drchal, and P. Bruno, Phys. Rev. B **64**, 174402 (2001).

[37] J. Mathon, Proc. R. Soc. London, Ser. A **306**, 355 (1968).

[38] J. Larrea J., M. B. Fontes, A. D. Alvarenga, E. M. Baggio-Saitovitch, T. Burghardt, A. Eichler, and M. A. Continentino, Phys. Rev. B **72**, 035129 (2005).

[39] M. A. Continentino, G. M. Japiassu, and A. Troper, Phys. Rev. B **39**, 9734 (1989).

[40] D. Belitz, T. R. Kirkpatrick, A. J. Millis, and T. Vojta, Phys. Rev. B **58**, 14155 (1998).

[41] This dependence of m on $(P - P_c)$ is valid in the clean system before the first-order transition and in the disordered ferromagnet, except extremely close to the quantum transition [18,40].

[42] G. R. Stewart, Rev. Mod. Phys. **56**, 755 (1984).

[43] I. Sheikin, Y. Wang, F. Bouquet, P. Lejay, and A. Junod, J. Phys.: Condens. Matter **14**, L543 (2002).

[44] N. Hessel Andersen and H. Smith, Phys. Rev. B **19**, 384 (1979); M. B. Fontes, J. C. Trochez, B. Giordanengo, S. L. Budko, D. R. Sanchez, E. M. Baggio-Saitovitch, and M. A. Continentino, *ibid.* **60**, 6781 (1999).

[45] F. Keffer, in *Encyclopedia of Physics: Ferromagnetism*, edited by H. P. J. Wijn (Springer, Berlin, 1966).

[46] B. Raquet, M. Viret, E. Sondergard, O. Cespedes, and R. Mamy, Phys. Rev. B **66**, 024433 (2002), and references therein.

[47] A. Steppke, R. Küchler, S. Lausberg, E. Lengyel, L. Steinke, R. Borth, T. Lühmann, C. Krellner, M. Nicklas, C. Geibel, F. Steglich, and M. Brando, Science **339**, 933 (2013).